

Gap and spin texture engineering of Dirac topological states at the Cr–Bi₂Se₃ interface

H. Aramberri¹ and M.C. Muñoz¹

¹*Instituto de Ciencia de Materiales de Madrid, ICMN-CSIC, Cantoblanco, 28049 Madrid, Spain.*

(Dated: October 6, 2018)

The presence of an exchange field in topological insulators reveals novel spin related phenomena derived from the combination of topology and magnetism. In the present work we show the controlled occurrence of either metallic or gapped topological Dirac states at the interface between ultrathin Cr films and the Bi₂Se₃ surface. The opening and closing of the gap at the Dirac point is caused by the spin reorientation transitions arising in the Cr films. We find that atom-thin layers of Cr adhered to Bi₂Se₃ surfaces present a magnetic ground state with ferromagnetic planes coupled antiferromagnetically. As the thickness of the Cr film increases stepwise from one to three atomic layers, the direction of the magnetization changes twice from out-of-plane to in-plane and to out-of-plane again. The out-of-plane magnetization drives the gap opening and the topological surface states acquire a circular meron spin structure. Therefore, the Cr spin reorientation leads to the metal-insulator transition in the Bi₂Se₃ surface and to the correlated modification of the surface state spin texture. Consequently, the thickness of the Cr film provides an effective and controllable mechanism to modify the metallic or gapped nature, as well as the spin texture of the topological Dirac states.

I. INTRODUCTION

The recent discovery of three dimensional (3D) topological insulators (TIs) has led to unique and fascinating physical phenomena, such as the quantum anomalous Hall (QAH) phase¹ and the topological magnetoelectric effect². The robustness of the surface metallicity under time reversal invariant perturbations and the realization of novel quantized states arising from their peculiar coupling to magnetic fields are distinct characteristics of this new phase of quantum matter. A central feature of TIs is the existence of helical surface states (SSs) with the electron spin locked to the crystal momentum^{3,4}. The presence in the TI of an exchange field, which violates time reversal symmetry (TRS), lifts the Kramers degeneracy and discloses novel spin related phenomena directly derived from the combination of topology and magnetism. The QAH effect has already been observed in three-dimensional magnetic TIs⁵. Nevertheless, the experimental realization of a magnetoelectric topological insulator, which in fact corresponds to a *non-integer* quantum Hall effect at the surface^{1,6}, still remains a challenge.

To experimentally achieve these topological phases a surface gapped by a TRS breaking perturbation is required. There are three different ways to break TRS in TIs, either by conventional doping with magnetic elements^{7–9}, by proximity to a magnetic film at a TI-magnetic interface^{10,11}, or by an external magnetic field¹². The effect of magnetic doping with 3d transition metals in the Bi₂Se₃ family of compounds has been extensively investigated both theoretically and experimentally^{7,9,13–19}. It has been shown that the interaction with magnetic impurities modifies the electronic and magnetic ground state of the 3D TIs. However, the changes in the ground state are not universal since they critically depend on the specific magnetic atoms, occupation sites of the magnetic impurities¹⁴, and experimental conditions.

Cr-doped Bi₂Se₃ is a prototype magnetic TI, and several works^{7,9,13–16} have reported magnetically induced effects in this system. First-principles calculations found that substitutional Cr, which is energetically more favorable than interstitial Cr, preserves the insulating character in the bulk and that Cr-doped Bi₂Se₃ is likely to be ferromagnetic^{20,21}. However, evidence from the experimental observations is so far inconclusive^{7,13,14,17–19}. Both ferro¹⁴ and antiferromagnetism⁷ have been reported and, recently, the coexistence of both ferro- and antiferromagnetic Cr defects in high quality epitaxial thin films has been observed²². Nevertheless, Cr doping of bulk or thin films of Bi₂Se₃ crystals seems to lead to a gap opening in the Dirac cone, evidencing time-reversal symmetry breaking^{7,13,14}. In contrast, surface deposition of Cr atoms on the surface of Bi₂Se₃ up to $\approx 10\%$ monoatomic layer (ML) coverages preserves the metallic surface²³. The absence of gap opening at the Dirac point indicates that for dilute Cr adatom concentrations there is no long-range out-of-plane ferromagnetic order. Despite these works, the interface between Cr films and the Bi₂Se₃ surface has not been investigated and thus the spin behavior of the topological SS under the interaction with ultrathin Cr films remains unknown.

In the present work we explore the spin configuration and topological state at the interface of Bi₂Se₃ surfaces and Cr films in the ultrathin limit, one to three MLs thick. We find that the presence of the Cr magnetic film triggers a double transition, from a Dirac-metal to a gapped system, on the topological SS of Bi₂Se₃ as a function of the Cr thickness. The gap opening at the Dirac point is induced by the proximity of the Cr film and thus the observed modulation of the gap is associated with the spin reorientation occurring in the magnetic layer. In fact, the magnetization direction in the Cr film evolves from out-of-plane to in-plane and once again to out-of-plane as the Cr thickness increases stepwise from one to two and three MLs. Correlated with the gap, there is

a modulation of the spin texture of the topological SSs, which undergoes a double circular skyrmion to circular meron transition.

II. MODEL AND METHODS

Density Functional Theory (DFT) spin-polarized calculations were carried out with the SIESTA code²⁴ as implemented in the GREEN package^{25,26}, although specific structures were also calculated with the Vienna *ab-initio* simulation package (VASP)²⁷. The generalized gradient approximation with Perdew-Burke-Ernzerhof²⁸ type exchange-correlation functional was used in all cases. In the SIESTA calculations, the spin-orbit coupling is considered via the recently implemented fully-relativistic pseudopotential formalism²⁶, while the semi-empirical pair-potential approach to van der Waals (vdW) forces of Ortmann *et al.*²⁹ was employed to correctly account for the weak inter quintuple layer (QL) interaction in the Bi₂Se₃ crystal. The numerical atomic orbitals basis set was generated according to the double ζ -polarized scheme with confinement energies of 100 meV. For the computation of three-center integrals, a mesh cut-off as large as 1200 Ry was used, equivalent to a real space grid resolution below 0.05 Å³. In the VASP calculations plane wave basis set with a kinetic energy cutoff of 340 eV was used. For the Brillouin zone (BZ) integrations a centered 13×13×1 k-sampling was employed, while the electron temperature was set to $k_B T=10$ meV in both calculation schemes.

Bi₂Se₃ has a rhombohedral crystal structure with space group R $\bar{3}m$ (D_{3d}⁵). It can be described as a layered compound constituted by QLs along the [0001] direction. A QL contains alternating Se and Bi atomic layers, and within each QL the two Bi layers are equivalent, while the Se in the middle is inequivalent to the external Se. The stacking pattern is *fcc*-like, -AbCaB-CaBcA-, where capital and small letters stand for Se and Bi, respectively. The Se-Bi bonds within the QLs are mainly covalent, while at adjacent QLs the Se-Se double-layer is only weakly bonded through van der Waals forces. The in-plane lattice parameter is $a_{\text{Bi}_2\text{Se}_3}=4.14$ Å, while $c=9.54$ Å determines the periodicity along the [0001] direction.

Bulk Cr follows a *bcc* crystal structure with lattice parameter $a_{\text{Cr}}=2.91$ Å. Each atom has 8 nearest neighbors (n.n.s). Surfaces perpendicular to the [111] direction exhibit three-fold C₃ symmetry and an open structure, since only 6 out of the 8 n.n.s lie in the adjacent atomic layers, while the remaining 2 n.n.s are located three atomic layers above and below. Along this direction the stacking sequence follows an ...ABCABC... pattern, analogous to that of the Bi₂Se₃ crystal in the [0001] direction (see Figure 1). Cr is unique among the 3d transition metals, showing an itinerant antiferromagnetic ground state. It exhibits a spin density (SDW) wave along the [100] direction –or, equivalently, along

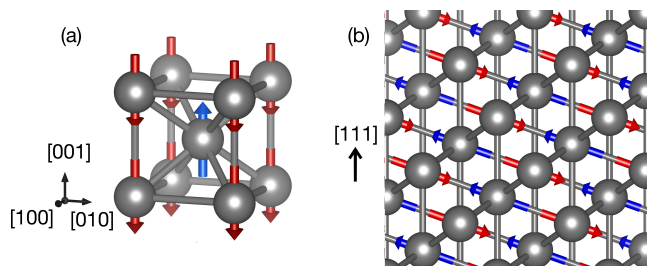


FIG. 1. (a) *bcc* unit cell of bulk Cr. Arrows indicate the magnetic moment. The two inequivalent atoms show opposite magnetic moment. (b) Side view of bulk Cr with the [111] direction as indicated in the figure. Cr exhibits an ABC stacking pattern along this direction, with opposite magnetic moments for alternating atomic planes. Two out of the eight first nearest neighbors of each atom lie in the first layer above and below, while the remaining six lie three layers above and below.

the [111] direction–, with a wave vector almost commensurate with the lattice, being its Néel temperature $T_N=311$ K. Contrary to what happens in bulk crystals, in which all three crystallographic directions are equivalent, in thin Cr films the SDW wave vector is perpendicular to the film surface and the SDW is commensurate with the lattice. Since the Cr–Bi₂Se₃ systems studied are formed of a maximum of 3 Cr layers, we can consider Cr as a pure antiferromagnet in the ultrathin film regime. Thus, the Cr slabs are expected to show atoms in the same atomic layer coupled ferromagnetically, being the interlayer coupling antiferromagnetic.

We model the Cr–Bi₂Se₃ interfaces by 1×1×1 and 2×1×1 supercells with the equilibrium in-plane lattice constant of bulk Bi₂Se₃. We take the [0001] Bi₂Se₃ direction as z and the (111) plane as the xy plane. Along the z direction the supercells contain the Cr film on top of either 4 or 6 QLs (20 or 30 atomic planes) of Bi₂Se₃ and a vacuum layer larger than 20 Å to avoid interaction between opposite surfaces. During the structure optimization, the Cr overlayers and the interfacemost QL of Bi₂Se₃ were fully relaxed until the residual forces were smaller than 0.02 eV/Å, while the remaining atoms were fixed to the relaxed geometry of the corresponding Bi₂Se₃ thin film.

III. ATOMIC STRUCTURE AND INTERFACE CHARGE TRANSFER

We consider commensurate Cr films with 1, 2 and 3 ML thicknesses on top of (111) Bi₂Se₃ surfaces. The atomic structure of the (111) composed slab exhibits three-fold C₃ symmetry and three reflection planes perpendicular to the surface –see Fig. 2 (a)–. The in-plane lattice parameters of Bi₂Se₃ (4.14 Å) and Cr (4.12 Å) show a small lattice mismatch of 0.5%. First, we examine different positions for the Cr overlayers, including *fcc* and *hcp* hollow sites, bridge and Se-top sites. As expected, the high

	Cr3-Cr2	Cr2-Cr1	Cr1-Se1	E_{ads}
1 ML	-	-	2.39	-2.00
2 ML	-	2.59	2.40	-1.98
3 ML	2.64	2.48	2.84	-1.77
3 ML-fcc*	3.11	3.42	2.39	-1.69

TABLE I. Relaxed bond lengths in Å between the Cr layers –columns 2 and 3– and between the interface Cr and the interface Se –column 4–. The last row corresponds to the more energetic *fcc* configuration (see Fig. 3) for the 3 ML Cr system. The adhesion energy E_{ads} is given in eV in the right-most column. The *fcc*-like case for the 3 ML Cr is more than 80 meV less stable.

symmetry hollow sites are the energetically most favorable. Figures 2 (a) to (d) show the calculated equilibrium structures. For 1 and 2 ML films the interfacial Cr atoms occupy the *fcc* hollow sites following the Bi_2Se_3 stacking, ...-BcAbC-**A** and ...-BcAbC-**AB** respectively, where bold letters correspond to Cr atoms. However, for the 3 ML film the interface Cr moves into the *hcp* hollow site on top of the Bi subsurface layer and there is a reversal of the stacking sequence³⁰, ...-BcAbC-**BAC**. This spatial self-organization of the Cr film has to be due to the peculiar open structure of the (111) *bcc* surface in which first n.n.s are in the adjacent layers and in the third layers above and below. In this way, while for the 1 and 2 ML Cr films the interface Cr atoms are almost coplanar to the surface Se and lie on top of the Se in the center of the first QL, for the 3 ML film the Cr-Se interface bond distance increases notably and the Cr at the interface lies on top of the outermost Bi. The relaxed bond lengths are given in Table I. The Cr-Cr distances are close to the bond lengths in bulk Cr, 2.49 Å. Note the increase in the Cr1-Se1 bond length for the 3 ML film. Additionally, the bond distances for the non-equilibrium Cr trilayer in the *fcc* configuration –see Fig. 3 (a)– are presented at the bottom of the Table. In this configuration, similar to the 1 and 2 ML cases, the interface Cr atoms remain almost coplanar to the Se surface at the expense of very large n.n.s Cr-Cr bond distances. The *fcc* configuration is about 80 meV more energetic than the equilibrium 3 ML Cr- Bi_2Se_3 structure, well above the energy involved in room temperature fluctuations.

The calculated binding energies are also given in the Table. The binding energy E_{ads} is obtained as

$$E_{\text{ads}} = E_{\text{Cr-Bi}_2\text{Se}_3} - E_{\text{Bi}_2\text{Se}_3} - E_{\text{Cr}} \quad (1)$$

where $E_{\text{Cr-Bi}_2\text{Se}_3}$ is the total energy for the composed Cr- Bi_2Se_3 system, $E_{\text{Bi}_2\text{Se}_3}$ is the total energy of the isolated 4 QL Bi_2Se_3 system and E_{Cr} is the total energy of the isolated Cr subsystem in the same ionic and magnetic configuration as it acquires in the composed Cr- Bi_2Se_3 system. We found a negative value for the adhesion energy for all the Cr films in correspondence with the exothermic character of dilute Cr adsorbed on Bi_2Se_3 surfaces for submonolayer coverages^{23,31}.

The different atomic configuration of the equilibrium structures is clearly reflected in the interface charge redistribution. We have calculated the Mulliken charges for the Cr- Bi_2Se_3 systems and for the corresponding isolated slabs, a pristine 4 QL Bi_2Se_3 slab, and the isolated Cr films of 1, 2 and 3 Cr MLs with the same atomic and magnetic configuration as they present when adhered to Bi_2Se_3 . The differences between the Mulliken charges of the entire Cr- Bi_2Se_3 systems and those corresponding to the isolated subsystems are displayed in Figure 4. In all the cases the charge transfer is small and mostly confined to the Cr film and the first Bi_2Se_3 QL. For 1 and 2 Cr ML coverages, the Cr layers acquire charge at the expense of the Se atoms, both at the interface and in the middle of the first QL. In the 3 Cr ML system, on the contrary, the charge transfer is towards the Bi_2Se_3 . The interfacial Cr donates charge, mainly to the n.n.s. Se, which gains electron charge, increasing its ionic radius and consequently increasing the interface bond length. This different behavior can be attributed to the different adsorption site of the first Cr layer (*hcp* hollow versus *fcc* hollow for 1 and 2 Cr MLs). Nevertheless, there is always a chemical interaction at the interface. In addition, the Bi_2Se_3 free surface presents a small charge gain in all the calculated structures.

IV. MAGNETIC GROUND STATE

To model the magnetic ground state of Cr layers we consider different configurations having parallel and antiparallel collinear Cr magnetizations both between planes and within a plane. We employed an in-plane unit cell with 2 atoms per plane. We find a ferrimagnetic ground state with ferromagnetic Cr planes coupled antiferromagnetically for all the studied Cr film thicknesses.

Due to the C_3 symmetry of both Cr and Bi_2Se_3 layers, the *3d* Cr and *4p* Se orbitals hybridize, as can be clearly appreciated in the spin-resolved total DOS for three Cr layers adhered to Bi_2Se_3 shown in Fig. 5. The hybridization drives the Cr states close to the Fermi level, confined in an energy region ≈ 1.5 eV below E_F . In addition, a large energy splitting of about 4 eV between the spin-majority and the spin-minority states is obtained, and the majority Cr states are fully occupied while the minority-spin channel is almost unoccupied. Therefore, the magnetic moments (MMs) of the Cr layers are close to the Hund rule value for isolated Cr atoms. The calculated MMs, shown in Table II, are remarkably large at the surface plane ($\geq 4 \mu_B/\text{atom}$) for all the systems, while they decrease for the subsurface Cr layers. For 1 and 2 ML Cr films there is an appreciable induced MM on the Se and Bi topmost planes of $0.2 \mu_B$, aligned opposite to the Cr MM at the interface, while the induced MMs in the Bi_2Se_3 for the 3 ML Cr film is almost negligible in correspondence with the different chemical interaction at the interface. Note the larger MMs of the 3 ML Cr *fcc* structure due to larger interlayer distances.

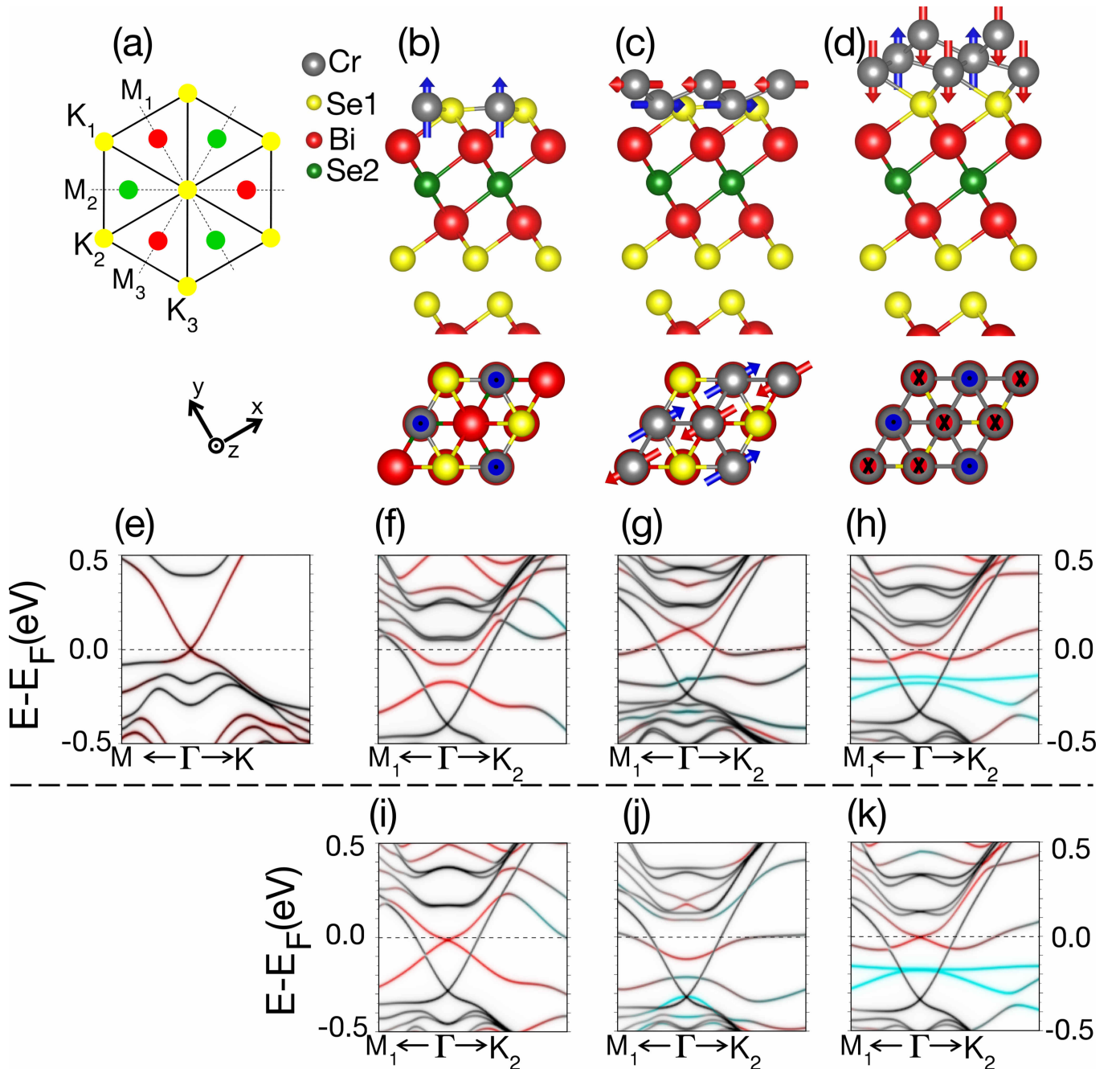


FIG. 2. (a) Top view of Bi_2Se_3 (111) surface. Dashed lines depict the mirror planes M_1 , M_2 and M_3 , and the M and K points of the Brillouin zone are also indicated. (b) to (d) show the relaxed geometries for 1 to 3 ML Cr coverages on a 4 QL Bi_2Se_3 slab, along with arrows indicating the magnetization of the Cr layers for the magnetic ground state in each case. (e) Band structure around the center of the Brillouin zone for a pristine 4 QL Bi_2Se_3 slab. (f) to (h) display the band dispersion diagrams for 1 to 3 Cr MLs on a 4 QL Bi_2Se_3 slab in the magnetic ground state configuration shown above. (i) to (k) Depict the band structure of 1 to 3 Cr MLs on a 4 QL Bi_2Se_3 slab with the Cr MMs perpendicular to that of the magnetic ground state for each system, *i.e.* along x for (i) and (k) and along z for (j). The projection of the states on the interfacemost QL of Bi_2Se_3 is shown in red, while the projection on the Cr subsystem is shown in cyan.

Since the spin-orbit coupling is included in the calculations we can determine the direction of the Cr MM relative to the crystal lattice. The preferential orientation of the Cr magnetization vector was obtained by comparing the total energies of in-plane (\mathcal{M}_x , \mathcal{M}_y) and

out-of-plane (\mathcal{M}_z) orientations of the total magnetization \mathcal{M} (the z axis is defined normal to the surface). It is noteworthy to point out that in the ground state within the planes the Cr atoms are always coupled ferromagnetically, thus the Cr MMs are aligned within each layer—see

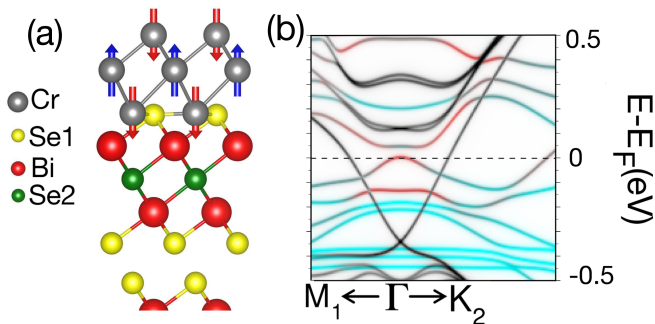


FIG. 3. (a) Side view of the 3 Cr ML on the Bi_2Se_3 (111) surface with the Cr layers following the stacking pattern of Bi_2Se_3 , i.e. with the first Cr layer occupying the *fcc* hollow site. The arrows indicate the magnetic ground state for this ionic configuration. Note that the ionic configuration shown in Fig. 2 (d) is more stable for the Cr trilayer. The band structure of a 4 QL Bi_2Se_3 slab with a Cr trilayer in the ionic and magnetic configuration depicted in (a) is shown in (b). The projection of the states on the interfacial QL of Bi_2Se_3 is shown in red, while the projection on the Cr subsystem is shown in cyan.

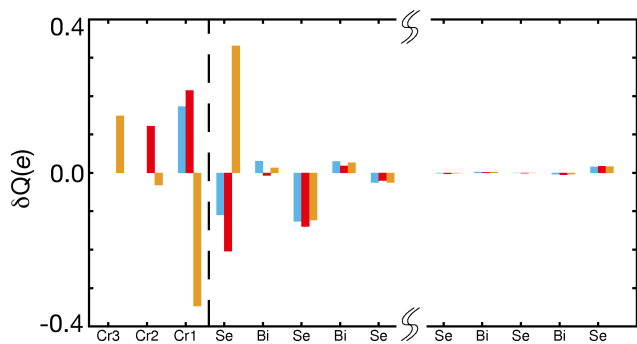


FIG. 4. Mulliken charge rearrangement of the 1 (cyan), 2 (red) and 3 (orange) Cr ML systems on a 4 QL Bi_2Se_3 slab. The figure displays the atomic charge difference between the isolated Cr and Bi_2Se_3 subsystems and that acquired in the composed Cr- Bi_2Se_3 system. Only the Cr subsystem and the first and last QLs are shown since the charge rearrangement in the inner QLs of Bi_2Se_3 is negligible. The Cr-Se interface is indicated with a dashed line as a guide to the eye.

	μ_{Cr3}	μ_{Cr2}	μ_{Cr1}	μ_{Tot}
1 ML	-	-	4.3	4.0
2 ML	-	4.2	-3.1	1.4
3 ML	-4.2	3.6	-3.7	-4.3
3 ML- <i>fcc</i> *	-4.9	4.7	-4.0	-3.8

TABLE II. Magnetic moments of the Cr layers in Bohr magnetons for 1, 2 and 3 ML coverages. Cr1 (Cr3) corresponds to the interfacial (farthest from the interface) Cr layer. μ_{Tot} is the total magnetization of the whole Cr- Bi_2Se_3 system for each case. The last row corresponds to the more energetic *fcc* configuration (see Fig. 3) for the 3 Cr ML system. Cr overlayers grow as a layer-by-layer ferrimagnet with in-plane ferromagnetic coupling.

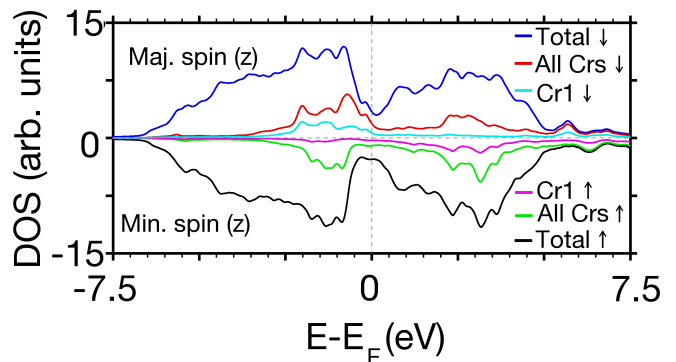


FIG. 5. Spin-resolved DOS for the Cr trilayer adhered to Bi_2Se_3 . The blue (black) line shows the majority (minority) spin total DOS, while the red (line) corresponds to the DOS projected on the whole Cr trilayer for the majority (minority) spin bands and the cyan (magenta) indicates the DOS projected on the interface-most Cr layer for the majority (minority) spin. Magnetism is patent from the difference in the majority and minority curves.

Fig. 2 (a)-.

The easy magnetization axis for the 1 ML Cr- Bi_2Se_3 system lies perpendicular to the surface (out-of-plane), while as the thickness of the Cr film increases a double spin reorientation transition takes place and the magnetization direction changes to in-plane for 2 ML and again to out-of-plane for the 3 ML Cr film. A similar spin reorientation transition has been reported in ultrathin Co films grown on hexagonal Ru (0001)³². The magnetic anisotropy for the 1 and 2 ML Cr- Bi_2Se_3 systems is unusually large, of ≈ 25 meV and 35 meV respectively, while for the 3 ML Cr- Bi_2Se_3 system we obtain a smaller value of 5 meV.

V. TOPOLOGICAL SURFACE STATES

We additionally analyze the electronic structure of the Cr- Bi_2Se_3 slabs. Figures 2 (e) to (h) show the corresponding band dispersions around the Γ point and that of the pristine Bi_2Se_3 4 QL film. The band dispersion of the pristine film shows the topologically protected metallic surface states with the Fermi level located at the Dirac point. However, for all the Cr- Bi_2Se_3 slabs the position of the Fermi level is shifted up between 0.2 and 0.4 eV with respect to the Dirac cone of the free Bi_2Se_3 surface, which persists in the three cases. As a result the free surface topological SSs are always electron doped.

Next, we focus on the SS when a single Cr overlayer is adhered to the Bi_2Se_3 surface. A large Dirac gap opens up, and the gap opening only occurs at the interface with the magnetic film while the Dirac cone at the free Bi_2Se_3 surface remains, evidencing the spatially localized character of the effect. Furthermore, our calculations reveal that the magnetic easy axis is along the out-of-plane direction as shown in Fig. 2 (b). Therefore, the origin of

the gapped Dirac point is the exchange coupling between the TI SS and the out-of-plane magnetization of the Cr film, which breaks TRS.

As explained above, in the 2 ML system the Cr layers present an in-plane magnetization, and we do not find any appreciable energy difference when the in-plane magnetization is along or normal to the vertical reflection planes of the Bi_2Se_3 thin films –see Figure 2 (a)–. Thus, we discuss the results for the in-plane magnetization normal to the reflection plane M_1 . The corresponding band dispersion around the Γ point is represented in Figure 2 (g). The topological surface state survives and there is no shift in momentum space of the Dirac point, which remains at Γ . However, the dispersion is no longer linear and the SS presents a large anisotropic mass. Only along the $-\text{K}_2-\Gamma-\text{K}_2$ line, perpendicular to the mirror plane, electrons at \mathbf{k} and $-\mathbf{k}$ have the same energy. The preservation of the Dirac point can be easily understood considering that although the breaking of TRS occurs for any non-zero magnetization, the slab is invariant under a reflection normal to the in-plane magnetization direction, thus the reflection symmetry M_1 survives. This result is a clear demonstration that in order to open a gap at the Dirac cone, breaking the TRS and the three reflection symmetries $M_{1,2,3}$ of the Bi_2Se_3 lattice is required³³. As in the 1 ML system, the Dirac cone at the free surface of Bi_2Se_3 remains unmodified but for an energy shift.

For the system consisting of 3 MLs of Cr on top of the Bi_2Se_3 thin film, the magnetization points again along the out-of-plane direction. Therefore, its behavior is analogous to that of the 1 Cr ML slab: a gap opens at the original Dirac point, although the gap is smaller. Moreover, it is worth to note that for 3 Cr MLs, the Fermi level lies exactly within the gap of the surface Dirac fermions gapped by the exchange interaction.

For comparison, we have additionally included the dispersion relations of the 1, 2 and 3 Cr- Bi_2Se_3 systems with the magnetization of the Cr layers aligned perpendicular to that of the corresponding magnetic ground states, *i.e.* in-plane along x for the 1 and 3 ML Cr and out-of-plane along z for the 2 ML Cr case –Fig. 2 (i) to (k)–. Now, the behavior of the topological SS is just the opposite, which confirms the correlation between the opening of the gap at the Dirac point and the presence of a perturbation that breaks both TRS and the invariance of the system under the three reflection symmetries of the Bi_2Se_3 lattice. The crossing of the topological SS persists whenever the magnetization is aligned in-plane and perpendicular to a reflection plane, as in the 1 and 3 Cr ML systems –Fig. 2 (i) and (k)–. In both cases the reflection symmetry M_1 is preserved. On the contrary, a gap opens for the out-of-plane 2 ML Cr film, where TRS and the three reflection symmetries $M_{1,2,3}$ are broken. The mass enhancement and the induced anisotropy in the topological SS for the 1 and 3 Cr MLs are also clearly appreciable. Moreover, the origin of the large calculated MAE is evident from the sharp contrast between the band structures of these excited states – Fig. 2 (i) to (k)– and their correspond-

ing magnetic ground states – Fig. 2 (f) to (h)–. Finally, the band structure of the non-equilibrium 3 ML Cr film with the *fcc* stacking is shown in Fig. 3 (b). As expected, there is a gap opening due to the out-of-plane magnetization, analogous to that developed in the equilibrium 3 ML Cr- Bi_2Se_3 structure –see Fig. 2 (h)–.

These results prove that the gap opening of the topological surface states is exclusively due to the interplay of the topology and the induced magnetization, and independent of the chemical behavior. As remarked above the 1 and 2 ML Cr- Bi_2Se_3 systems show similar interface chemical interactions –the charge transfer has the same sign and similar value– and opposite to the interface interaction in the 3 ML slab (see Figure 4). Nevertheless, there is a gap in the 1 and 3 ML Cr- Bi_2Se_3 systems, while in the 2 ML Cr- Bi_2Se_3 structure the degeneracy of the topological SS at the Γ point remains.

VI. SPIN TEXTURE OF THE SURFACE STATES

As shown above, the magnetization of the Cr layers attached to the surface of the Bi_2Se_3 film provides a local magnetic field, which modifies the degeneracy and topology of the SS. Additionally, it induces a spin component along the magnetization direction and alters the spin texture of the topological SS. We examine the spin texture of the SSs in the equilibrium Cr- Bi_2Se_3 systems close to Γ by calculating the expected value of the spin operator. The results are displayed in Figure 6, which also includes the spin distribution of the Dirac cone states of the pristine Bi_2Se_3 surface. For the latter the spin is locked perpendicular to crystal momentum, showing the distinct helical spin texture protected by TRS, and S_z vanishes close to the Dirac point. At large k there is, however, a finite small S_z component due to the trigonal warping. S_z remains null along the mirror lines Γ -M and reverses its sign traversing from K to -K, in correspondence with the trigonal symmetry of the system.

The spin texture of the gapped topological SSs (1 and 3 ML Cr systems) is in sharp contrast to that of the free surface. In the vicinity of the gapped Dirac point, the states show an imbalance between S_z and $-S_z$ at a given energy, and they present a significant net out-of-plane spin polarization. Only the in-plane components reverse sign changing from \mathbf{k} to $-\mathbf{k}$. Furthermore, the upper and lower Dirac bands have opposite S_z , evidencing that the spin degeneracy is indeed lifted at the Γ point. For larger \mathbf{k} , away from Γ , the induced S_z component gradually decreases, and the out-of-plane spin distribution results from the competition between the magnetic order that aligns the spin along the out-of-plane direction and the spin texture imposed by the warping term which forces adjacent K points to have opposite S_z . In the 2 ML Cr slab, the in-plane magnetization exhibited by the Cr layers in the interfacial plane does not induce observable spin reorientations of the Dirac state, and its spin texture

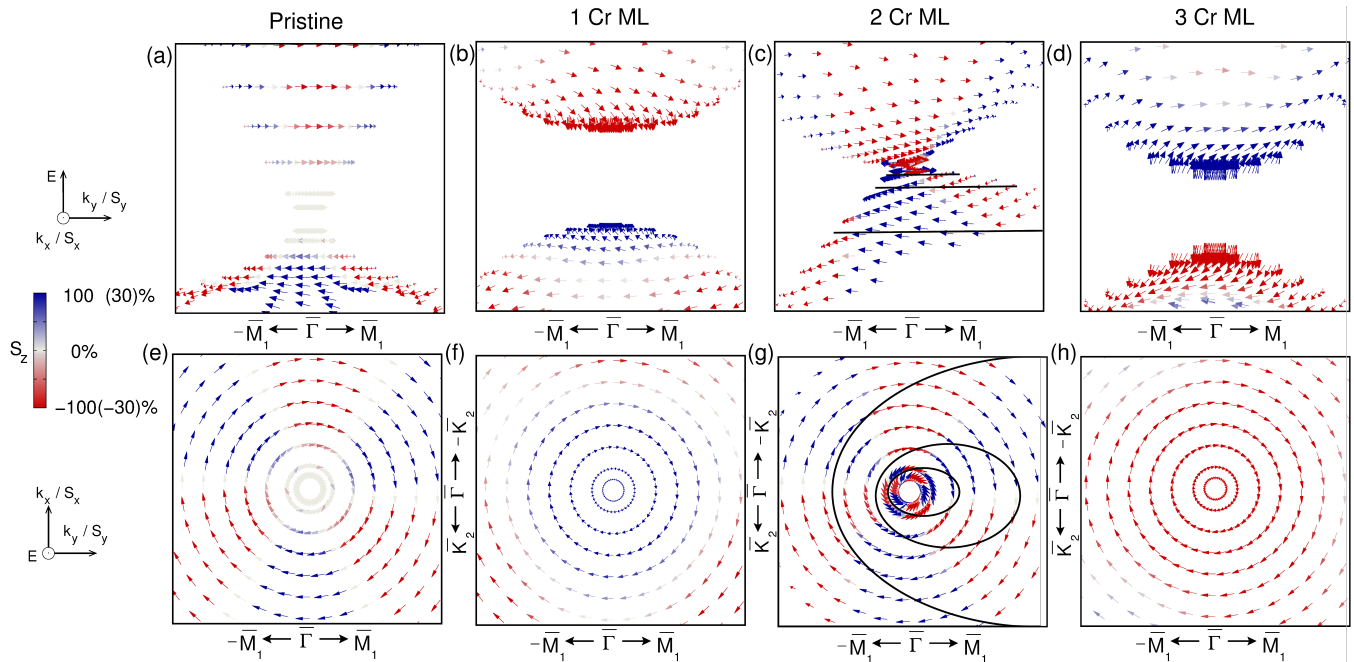


FIG. 6. (a) to (d): Side view of the spin texture of the surface state for Cr overlayers of 0 (pristine Bi_2Se_3 surface) to 3 MLs. (e) to (h): Top view of the hole-like surface state for Cr coverages of 0 to 3 MLs. The expectation value for the spin is shown as an arrow at each k -point, while the S_z component is additionally color coded according to the scale at the right, being the limits ± 100 (30)% of the modulus of $S = \sqrt{S_x^2 + S_y^2 + S_z^2}$ for the 1 and 3 (0 and 2) Cr MLs. In the 2 Cr ML system (c) and (g)– three elliptical black solid lines depict constant energy contours. The circular meron texture is patent in the 1 and 3 ML cases, while the spin texture of the 2 Cr MLs on Bi_2Se_3 is an anisotropic circular skyrmion.

is analogous to that of the free surface Dirac cone. However, due to the large anisotropy of the effective mass, the constant energy lines are no longer circular, but present an elliptical shape. Nevertheless, the SSs exhibit a well defined spin helicity and the total spin cancels in every constant energy contour. TRS breaking is evident from the spin texture of the three Cr- Bi_2Se_3 systems analyzed.

VII. CONCLUSIONS

In summary, we have found that the structural configuration of ultrathin Cr films attached to the (111) surface of Bi_2Se_3 is determinant to establish the topological behavior of Bi_2Se_3 SSs. Due to the coupling between Cr $3d$ orbitals and the Bi_2Se_3 electrons, the Cr interface induces simultaneous charge and magnetic doping. However, the properties of the topological SS critically depend on the Cr film thickness and are independent of the specific chemical interaction at the Cr- Bi_2Se_3 interface. As the thickness of the Cr film increases stepwise from one to three MLs, the magnetization of the Cr layers undergoes two reorientation transitions, and changes from out-of-plane (1 ML) to in-plane (2 ML) and to out-of-plane (3 ML) once again. For the 1 ML and 3 ML Cr- Bi_2Se_3 interfaces the magnetic overlayer induces

a gap at the Dirac point, producing massive fermions at the interface. Moreover, the gap already opens for a single Cr ML, and the value of the gap depends on the absolute value of the exchange interaction. In contrast, for the 2 ML Cr system the gapless Dirac cone is preserved. The complexity of the spin texture of gapped Dirac states signifies a competition between the in-plane helical component of the spin dictated by the spin-orbit coupling and the out-of-plane TRS breaking component induced by the proximity to the magnetic Cr. Our results evidence the importance of the actual structural configuration of the magnetic films and show that the thickness of the Cr film can be used to modify in a controlled way the metallic or gapped nature of topological Dirac states and their associated spin texture.

ACKNOWLEDGMENTS

This work has been supported by the Spanish Ministry of Economy and Competitiveness through Grants MAT2012-38045-C04-04 and MAT2015-66888-C3-1-R. We acknowledge the use of computational resources of CESGA, Red Española de Supercomputación (RES) and the i2BASQUE academic network. We also acknowledge J.I. Cerdá for fruitful discussions.

- ¹ R. Yu, W. Zhang, H.-J. Zhang, S.-C. Zhang, X. Dai, and Z. Fang, *Science* **329**, 61 (2010).
- ² X.-L. Qi, T. L. Hughes, and S.-C. Zhang, *Phys. Rev. B* **78**, 195424 (2008).
- ³ H. Zhang, C.-X. Liu, X.-L. Qi, X. Dai, Z. Fang, and S.-C. Zhang, *Nature Physics* **5**, 438 (2009).
- ⁴ W. Zhang, R. Yu, H.-J. Zhang, X. Dai, and Z. Fang, *New Journal of Physics* **12**, 065013 (2010).
- ⁵ C.-Z. Chang, J. Zhang, X. Feng, J. Shen, Z. Zhang, M. Guo, K. Li, Y. Ou, P. Wei, L.-L. Wang, *et al.*, *Science* **340**, 167 (2013).
- ⁶ A. M. Essin, J. E. Moore, and D. Vanderbilt, *Phys. Rev. Lett.* **102**, 146805 (2009).
- ⁷ Y. H. Choi, N. H. Jo, K. J. Lee, J. B. Yoon, C. Y. You, and M. H. Jung, *Journal of Applied Physics* **109**, 07E312 (2011).
- ⁸ Y. S. Hor, P. Roushan, H. Beidenkopf, J. Seo, D. Qu, J. G. Checkelsky, L. A. Wray, D. Hsieh, Y. Xia, S.-Y. Xu, D. Qian, M. Z. Hasan, N. P. Ong, A. Yazdani, and R. J. Cava, *Phys. Rev. B* **81**, 195203 (2010).
- ⁹ J. J. Cha, J. R. Williams, D. Kong, S. Meister, H. Peng, A. J. Bestwick, P. Gallagher, D. Goldhaber-Gordon, and Y. Cui, *Nano Letters* **10**, 1076 (2010).
- ¹⁰ W. Qin and Z. Zhang, *Phys. Rev. Lett.* **113**, 266806 (2014).
- ¹¹ W. Liu, L. He, Y. Xu, K. Murata, M. C. Onbasli, M. Lang, N. J. Maltby, S. Li, X. Wang, C. A. Ross, P. Bencok, G. van der Laan, R. Zhang, and K. L. Wang, *Nano Letters* **15**, 764 (2015).
- ¹² M. Sitte, A. Rosch, E. Altman, and L. Fritz, *Phys. Rev. Lett.* **108**, 126807 (2012).
- ¹³ Y. L. Chen, J.-H. Chu, J. G. Analytis, Z. K. Liu, K. Igarashi, H.-H. Kuo, X. L. Qi, S. K. Mo, R. G. Moore, D. H. Lu, M. Hashimoto, T. Sasagawa, S. C. Zhang, I. R. Fisher, Z. Hussain, and Z. X. Shen, *Science* **329**, 659 (2010).
- ¹⁴ P. P. J. Haazen, J.-B. Laloë, T. J. Nummy, H. J. M. Swagten, P. Jarillo-Herrero, D. Heiman, and J. S. Moodera, *Applied Physics Letters* **100**, 082404 (2012).
- ¹⁵ C.-Z. Chang, P. Tang, Y.-L. Wang, X. Feng, K. Li, Z. Zhang, Y. Wang, L.-L. Wang, X. Chen, C. Liu, W. Duan, K. He, X.-C. Ma, and Q.-K. Xue, *Phys. Rev. Lett.* **112**, 056801 (2014).
- ¹⁶ J. J. Cha, M. Claassen, D. Kong, S. S. Hong, K. J. Koski, X.-L. Qi, and Y. Cui, *Nano Letters* **12**, 4355 (2012).
- ¹⁷ A. I. Figueroa, G. van der Laan, L. J. Collins-McIntyre, S.-L. Zhang, A. A. Baker, S. E. Harrison, P. Schönherr, G. Cibin, and T. Hesjedal, *Phys. Rev. B* **90**, 134402 (2014).
- ¹⁸ X. F. Kou, W. J. Jiang, M. R. Lang, F. X. Xiu, L. He, Y. Wang, Y. Wang, X. X. Yu, A. V. Fedorov, P. Zhang, and K. L. Wang, *Journal of Applied Physics* **112**, 063912 (2012).
- ¹⁹ X. Kou, L. He, M. Lang, Y. Fan, K. Wong, Y. Jiang, T. Nie, W. Jiang, P. Upadhyaya, Z. Xing, Y. Wang, F. Xiu, R. N. Schwartz, and K. L. Wang, *Nano Letters* **13**, 4587 (2013).
- ²⁰ J.-M. Zhang, W. Zhu, Y. Zhang, D. Xiao, and Y. Yao, *Phys. Rev. Lett.* **109**, 266405 (2012).
- ²¹ J.-M. Zhang, W. Ming, Z. Huang, G.-B. Liu, X. Kou, Y. Fan, K. L. Wang, and Y. Yao, *Phys. Rev. B* **88**, 235131 (2013).
- ²² W. Liu, D. West, L. He, Y. Xu, J. Liu, K. Wang, Y. Wang, G. van der Laan, R. Zhang, S. Zhang, and K. L. Wang, *ACS Nano* **9**, 10237 (2015).
- ²³ E. Wang, P. Tang, G. Wan, A. V. Fedorov, I. Miotkowski, Y. P. Chen, W. Duan, and S. Zhou, *Nano Letters* **15**, 2031 (2015).
- ²⁴ J. M. Soler, E. Artacho, J. D. Gale, A. García, J. Junquera, P. Ordejón, and D. Sánchez-Portal, *Journal of Physics: Condensed Matter* **14**, 2745 (2002).
- ²⁵ J. I. Cerdá, M. A. Van Hove, P. Sautet, and M. Salmeron, *Phys. Rev. B* **56**, 15885 (1997).
- ²⁶ R. Cuadrado and J. I. Cerdá, *Journal of Physics: Condensed Matter* **24**, 086005 (2012).
- ²⁷ G. Kresse and J. Hafner, *Phys. Rev. B* **48**, 13115 (1993).
- ²⁸ J. P. Perdew, K. Burke, and M. Ernzerhof, *Phys. Rev. Lett.* **77**, 3865 (1996).
- ²⁹ F. Ortman, F. Bechstedt, and W. G. Schmidt, *Phys. Rev. B* **73**, 205101 (2006).
- ³⁰ H. Aramberri, J. I. Cerdá, and M. C. Muñoz, *Nano Letters* **15**, 3840 (2015).
- ³¹ L. B. Abdalla, L. Seixas, T. M. Schmidt, R. H. Miwa, and A. Fazzio, *Phys. Rev. B* **88**, 045312 (2013).
- ³² F. El Gabaly, S. Gallego, C. Muñoz, L. Szunyogh, P. Weinberger, C. Klein, A. K. Schmid, K. F. McCarty, and J. de la Figuera, *Phys. Rev. Lett.* **96**, 147202 (2006).
- ³³ X. Liu, H.-C. Hsu, and C.-X. Liu, *Phys. Rev. Lett.* **111**, 086802 (2013).